International Journal of Mechanical, Industrial and Aerospace Sciences
ISSN: 2517-9950
Vol:10, No:10, 2016

Limits of Phase Modulated Frequency Shifted Holographic Vibrometry at Low Amplitudes of Vibrations

Pavel Psota, Vít Lédl, Jan Václavík, Roman Doleček, Pavel Mokrý, Petr Vojtíšek

***Abstract*—**This paper presents advanced time average digital holography by means of frequency shift and phase modulation. This technique can measure amplitudes of vibrations at ultimate dynamic range while the amplitude distribution evaluation is done independently in every pixel. The main focus of the paper is to gain insight into behavior of the method at low amplitudes of vibrations. In order to reach that, a set of experiments was performed. Results of the experiments together with novel noise suppression show the limit of the method to be below 0.1 nm.

***Keywords*—**Acousto-optical modulator, digital holography, low amplitudes, vibrometry.

I. Introduction

THE pioneering work in in the field of time average holography was done by Powell and Stetson [1], [2] that dates back to 1965. They were followed by many researches who have been improving the technique. Goodman [3] followed by important work of Aleksoff [4] made the first steps in extension of time average holographic interferometry measurement range by means of frequency shift. The detectable smallest amplitude with frequency shift was estimated by Ueda et al. [5] to be $2.7\times10^{-4}\lambda$. Time average holography has significantly changed after the beginning of the digital era. Picard et al. [6] captured time averaged digital hologram with a digital CCD camera. It was the beginning of time average digital holography (TADH). The use of acousto-optical modulators was introduced by Clerc et al. [7]. Further, Joud et al. [8] employed acousto-optical modulators in TADH for large amplitudes measurement while Psota et al. [9] applied frequency shift for very small amplitudes. Other configuration with great sensitivity for small amplitudes was presented by Verrier [10].

One of the most important tasks in time-average holography is to qualitatively determine the amplitude distribution from the fringe pattern modulated by Bessel function. Direct inversion of intensity to amplitude map was applied by Borzsa [11] and Psota et. al in [9]. However, due to not monotonous behavior of Bessel function, the procedure is only valid for very small amplitudes. Progress was made by Stetson and Brohinski [12] who placed a PZT mirror in reference arm of the holographic arrangements in order to alter its phase and shift the Bessel fringes similarly to phase stepping in case of cosine fringes. Psota et al. [13] applied Bragg cells in experimental arrangements in order to modulate the both phase and frequency of the reference wave, which resulted in quantitative measurement of amplitudes of vibrations independently in every single pixel with extended dynamic range. This method can be called phase modulated frequency shifted time average digital holography (PMFSTADH). This paper introduces a way of data processing that helps to suppress speckle noise. Another aim is to experimentally establish the low limit of measurable amplitudes of vibration by this method.

P. Psota, V. Lédl, R. Doleček, P. Vojtíšek are with the Regional Centre for Special Optics and Optoelectronic Systems (TOPTEC), Institute of Plasma Physics, Academy of Sciences of the Czech Republic, Za Slovankou 1782/3, 182 00 Prague 8, Czech Republic (e-mail: psota@ ipp.cas.cz)

J. Václavík and P. Mokrý are with the Institute of Mechatronics and Computer Engineering, Technical University of Liberec, Studentska 2, 4117 Liberec, Czech Republic (e-mail: pavel.mokry@tul.cz).

This work has been supported by Czech Science Foundation Project No.: GACR GA16-11965S.

II. Holographic Vibrometry

A. Digital Holography

Digital holography consists of two steps. Firstly, a digital hologram is recorded as a superposition of wave scattered from the object and reference wave. The digital hologram is sampled by a CCD or CMOS with pixel extensions $\xi \times \eta$ and transferred to a computer as an array of numbers. Further, the digital hologram must be numerically reconstructed. The propagation of optical fields is completely described by diffraction theory, which allows numerical reconstruction of the digital hologram $H(\xi,\eta)$ by multiplication with a numerical model of the reference wave $r(\xi,\eta)$ and propagation of the complex field from a hologram plane to an image plane at distance *d*. For a planar reference wave, we can put $r(\xi,\eta)=1$. The propagation of the wave field behind the digital hologram can be computed by Fresnel transform describing complex field $U(x,y)$ at an image plane with coordinates *x, y* by:

$$U(x,y)=\frac{j}{\lambda d}\exp\left(-\frac{j\pi}{\lambda d}\left[x^2+y^2\right]\right)\times \\ \times\,\Im^{-1}\left\{H(\xi,\eta)r^*(\xi,\eta)\exp\left(-\frac{j\pi}{\lambda d}\left[\xi^2+\eta^2\right]\right)\right\}. \quad (1)$$

In (1) $\Im^{-1}$ denotes the inverse discrete Fourier transform, *j* denotes complex number and λ is wavelength of the used

laser. Intensity distribution and phase distribution can be determined from the complex wave field as:

$$I(x,y)=|U(x,y)|^2,\qquad \varphi(x,y)=a\tan\frac{\mathrm{Im}\{U(x,y)\}}{\mathrm{Re}\{U(x,y)\}}. \tag{2}$$

B. Time Average Digital Holography

If the object oscillates harmonically with the amplitude of vibration: $d(x,y,t)=d(x,y)\sin\omega t$ at angular frequency ω, phase of the scattered wave is modulated. Holographical recording of such an oscillating object with an exposure time much longer when compared to the period of the vibration of the object results in intensity of the reconstructed image proportional to square of the first kind zero-order Bessel function J_0:

$$I(x,y)=|U_0(x,y)|^2 J_0{}^2(\Omega(x,y)), \tag{3}$$

where $|U_0(x,y)|^2$ represents intensity distribution of the object in steady state. In other words, the intensity of the reconstructed intensity map is modulated by the Bessel function. In (3) the argument of the Bessel function $\Omega(x,y)=d(x,y)e(x,y)$ is a product of amplitude of the vibration and sensitivity vector *e(p),* which is defined by the geometry of the holographic arrangement. This method is called TADH.

The range of measureable amplitudes of vibrations by the method is limited from the both sides. In order to examine the sensitivity of time average holography for small amplitudes, we can rewrite the Bessel functions as the power series:

$$J_n(\Omega)=\sum(-1)^i\Omega^{n+2i}/\left(2^{n+2i}i!(n+i)!\right) \tag{4}$$

that holds for $|\Omega|<\infty$. For very small amplitudes $\Omega\to 0$ and the sensitivity of time average method is approaching zero:

$$\lim_{\Omega\to 0}\frac{dJ_0(\Omega)}{d\Omega}=0 \tag{5}$$

Therefore, TADH cannot be used for measurement of very small amplitudes of vibration. Moreover, a retrieval of amplitude distribution from (3) is also very challenging. These drawbacks can be addressed by phase modulated frequency shifted TADH (PMFSTADH), where the frequency of the reference wave is shifted by an integer multiple $n\omega$ of the object vibration frequency ω and its phase is modulated at the frequency ω of the vibrating object with a modulation depth of B:

$$f_{ref}(t)=\exp(jn\omega t)\exp(jB\sin(\omega t)) \tag{6}$$

and magnitude of the reconstructed field (3) becomes [14]:

$$|U(x,y)|=|U_0(x,y)|J_n(\Omega(x,y)-B) \tag{7}$$

Now one can control the order of the Bessel function and its argument loci. In time average holography with no modulation, the magnitude of reconstructed field $|U|\approx|J_0(0)|$ is unity and has zero slope, see (5). On the other hand, when *n=1*, $|U|\approx|J_1(0)|$ has a positive slope in the dark field:

$$\lim_{\Omega\to 0}\frac{dJ_1(\Omega)}{d\Omega}=0.5 \tag{8}$$

yielding visible intensity variations even for small amplitudes. Moreover, the loci of bright zero fringes are controllable by the user, since they appear where $\Omega(p)=B$. This feature can be used for employment of phase shifting technique [12] leading to easy and accurate amplitude distribution retrieval [13].

C. Noise Suppression

The reconstructed magnitude distribution of TADH (or PMFSTADH) is multiplied by the low frequency background intensity caused by a varying illumination $|U_0|$. Moreover, noise sources like electronic noise, modulation of the interference pattern (digital hologram), speckle noise, dust particles, environmental distortions are presented. All the aforementioned mentioned distortions affect the additive A and multiplicative M noise components and therefore (7) can be rewritten in a form:

$$|U_{Jn}(x,y)|=A+M|J_n(\Omega(x,y)-B)|. \tag{9}$$

Note that using of term U_{Jn} in (9) instead of U in (7) is from clarity reason in following equations. The additional component A is eliminated due to phase-shifting but the influence of the multiplicative noise should be treated. The most significant source of noise is deterministic speckle noise described by phase Ω_S. The speckles are characterized by high-spatial frequency and due to their deterministic nature they cannot be easily removed. The direct approach to a complex field within digital holography, however, enables to lower the speckle noise. For that one needs to use two digitally reconstructed time-averaged holograms: one of the vibrating objects $\sim U_{Jn}$ and the other object at the steady state $\sim U_S$. The reconstructed complex field (valid for oscillating as well as steady state) $U=Re\{U\}+jIm\{U\}$ by formulas consists of orthogonal components (real and imaginary part). Let us consider complex field of the object without oscillations U_S and of the object undergoing harmonically oscillations U_{Jn}:

$$U_S(x,y)=M_0\exp[j(\Omega_S+\Omega_{D0})] \tag{10}$$

$$U_{Jn}(x,y)=M_1\exp[j(\Omega_S+\Omega_{D1})]J_n(\Omega(x,y)-B). \tag{11}$$

respectively. Normalization of (11) with respect to (10) is calculated as a product of complex field U_{Jn} and conjugate of U_S divided by envelope $|U_S|$:

$$\left\langle \frac{U_{Jn}(x,y)U_s^{*}}{\left|U_s^{2}\right|} \right\rangle = \frac{M_1}{M_0}\exp\left[j(\Omega_{D1}+\Omega_{D0})\right]J_n(\Omega(x,y)-B). \quad (12)$$

It is important to notice, that in (12) the high spatially varying speckle noise Ω_S is replaced by low frequency phase drift $\Delta\Omega_D = \Omega_{D1} - \Omega_{D0}$ between the measurements of U_s and U_{Jn}. Therefore, the time gap between the measurements is required to be minimized. Moreover, the smooth orthogonal components of $U_{Jn}U_s^{*}/|U_s|^2$ can be easily low-pass filtered without the loss of fringe contrast, see Fig. 1. The filtering process removing the high-frequency speckle noise is denoted by the symbol $\langle\ \rangle$. Considering $\Delta\Omega_D \approx 0$ and $M_1 \approx M_2$, the reconstructed magnitude of complex field (12) becomes:

$$|U_{Jn}(x,y)| \approx |J_n(\Omega(x,y)-B)|. \quad (13)$$

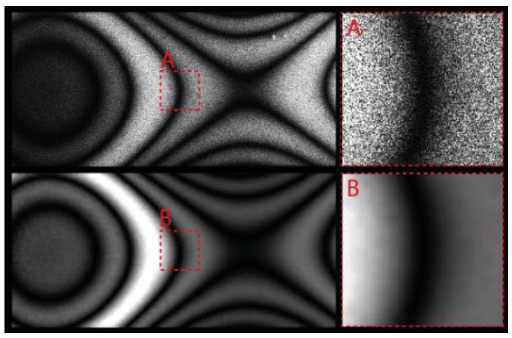

Fig. 1 Non filtered magnitude distribution (a) and its filtered version (b). Detailed subsections of the both versions are shown in the right column

III. Experiments and Results

Fig. 2 outlines the Mach-Zehnder type of holographic interferometer used for the measurement. The laser beam has a wavelength of 532 nm and a power of 150 mW. Behind the mechanical shutter, the beam is split in two by the polarizing beam splitter equipped with half-wavelength retardation plates. Half-wavelength retardation plates help to set the intensities in both beams as well as the polarization of each beam. The first beam acts as a reference wave and it could be further attenuated if necessary by a set of gray filters placed in the filter wheels. Each beam is frequency-shifted by means of an acousto-optic frequency modulator - Bragg cell with a fundamental frequency of 40 MHz. Moreover the heterodyne detection [7]-[9] and phase modulation according to (6) was employed. The both beams are further spatially filtered and collimated. After two reflections on mirrors M2 and M3, the reference beam hits CCD. The object beam illuminates the sample and the light scattered from its surface impinges on the CCD sensor. The setup is designed as in line scheme. The camera is an AVT Stingray - F 504 with a resolution of 2045 × 2056 pixels, each pixel having the size 3.45 μm × 3.45 μm. The camera is connected to the computer via a Fire Wire B interface enabling a frame rate of 6.5 FPS. The image from the camera – digital hologram – is cropped to 2048 × 2048 pixels due to Fast Fourier Transform (FFT) in the reconstruction process. A sequence of 16 phase-shifted frames was captured and processed in a way presented in section I and II.

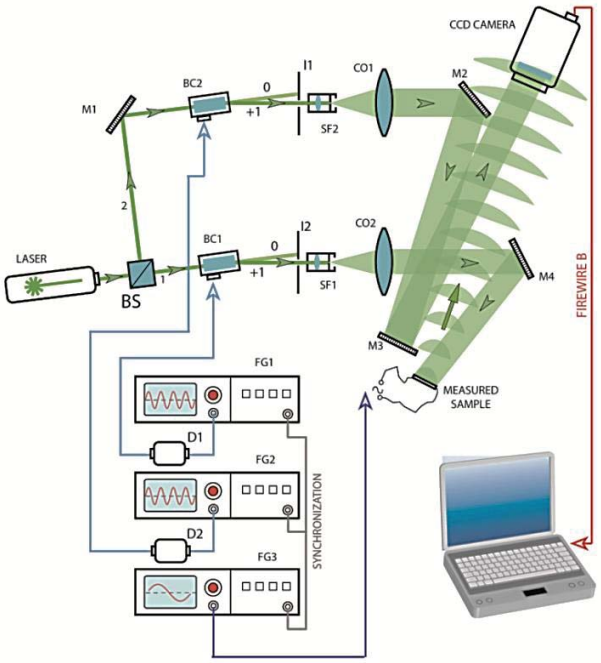

Fig. 2 Outline of the experimental arrangement used for cantilever measurement employing components: BS – beam splitter, SF – spatial filter, BC – Bragg cell, M – mirror, CO – collimating objective, FG – function generator, D – driver

The following experiment comprises two aims. The first aim is to verify validity of (7). The second aim is to compare sensitivity of frequency modulated with frequency non-modulated TADH for small amplitudes. The experiment was conducted with oscillating cantilever at frequency $f = \omega/2\pi = 6000\,Hz$ supplied with different values of voltage. Properties of such a cantilever require linear behavior in every single pixel: increasing supplying voltage u leads to proportional increase of maximal amplitude of vibrations $d_Z = C_v u$ with proportional constant C_v. Starting with non-modulated measurement; both Bragg cells were only driven by harmonic signal with working RF frequency $f_o = f_r = f_0 = 40\,MHz$. Therefore, frequency of both wavefronts is shifted about the same value f_0 and no frequency modulation is employed. A set of ten digital holograms with different supplying voltages was captured and reconstructed using Fresnel transform. The magnitude of the reconstructed complex field in the image plane $|U_{J0}| \approx \left|J_0\left(\frac{4\pi}{\lambda}C_v u\right)\right|$ holds for arrangements with parallel illumination and observation. The reconstructed magnitude images are introduced in the left column of the black frame in Fig. 3. The very top image represents magnitude distribution measured at supply voltage $u = 0.05\,V$. Lower images show how the magnitude distributions vary with increasing voltage of step $\Delta u = 0.05\,V$ up to $u = 0.5\,V$. As expected, higher voltage applied on the

cantilever results in its larger vibration amplitudes and growing number of dark fringes in the magnitude field.

The same procedure, except the Bragg cells driven signal settings, was repeated for frequency modulated time average holography. In this case, the Bragg cell in the reference arm was driven by harmonic signal having frequency $f_r = f_0 + f_{R-mod} = f_0 + nf$, where $n = 1$ and thus $f_r = 40.006\,MHz$. The wave-front of the object wave remains modulated only at working frequency $f_o = f_0 = 40\,MHz$. Resulting magnitude distributions $|U_{J1}| \approx \left|J_1\left(\frac{4\pi}{\lambda}C_v u\right)\right|$ are modulated by 1st order Bessel function and organized with the same logic as in the previous case in the right column of the black frame in Fig. 3. Similarly, we can observe the growing number of dark fringes when the supply voltage increases.

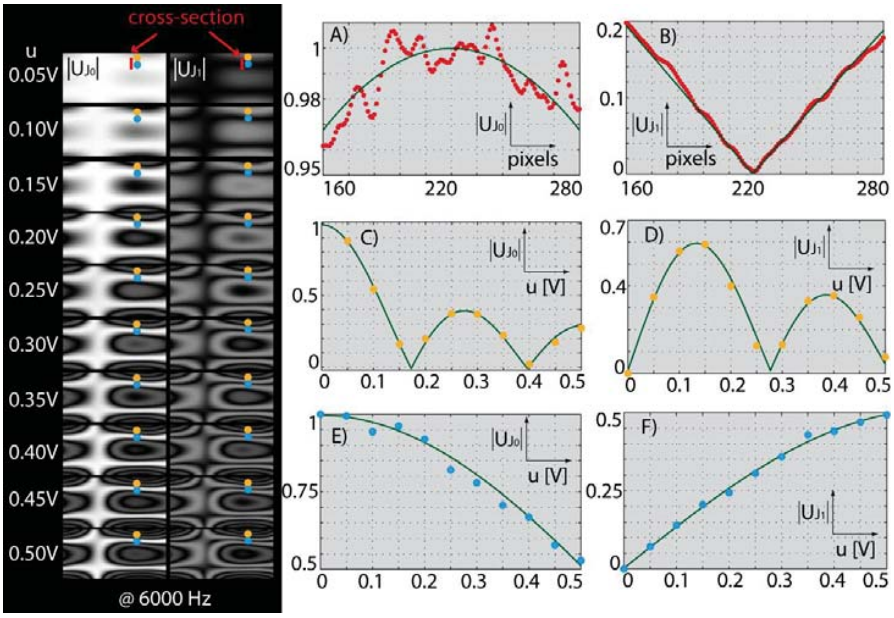

Fig. 3 (Black frame) Impact of frequency modulation on magnitude maps when increasing the supply voltage; (A, B). Measured values (red points) and theoretical values (green line) along cross-section denoted by the red line in magnitude map for 0.05V. Left plot (A) stands for non-modulated holography, where the sensitivity and SNR is obviously lower when compared to modulated technique introduced in the right plot (B); (C, D, E, F) As the supply voltage increases, the magnitude in each pixel varies. Magnitude variations at two pixels denoted by orange and blue circle were investigated in detail and compared to theoretical curves (green line). This was done for non-modulated (C, D) as well as modulated (D, F) technique

Two representative pixels from the magnitude distributions were picked for further analysis. The first pixel denoted by an orange circle ("orange point") is relatively far from the nodal line, while the second pixel denoted by a blue circle ("blue point") is closer. Since the orange point is far from the nodal line and so closer to antinode, the amplitude of vibration is more sensitive to supply voltage than in the case of the blue point. The development of magnitude distributions $|U_{J0}|$, and $|U_{J1}|$ as a function of the supply voltage, are plotted in the middle and down plots in Fig. 3. The discrete values (blue or orange points) are measured values, while the solid line represents the theoretically derived function $\left|J_0\left(\frac{4\pi}{\lambda}C_v u\right)\right|$, $\left|J_1\left(\frac{4\pi}{\lambda}C_v u\right)\right|$, respectively. One can see that the measured points in both measurement modes (non-modulated and modulated) follow the predicted curves described by the Bessel function of corresponding order. The proportional constant C_v was set to be an optimization parameter found by means of least square fitting. Obviously, the proportional constant obtained from $|U_{J0}|$ and $|U_{J1}|$ in the same point must be in agreement. For the orange point, the fitted procedure returns the proportional constant $C_v = 589$ in the case of $|U_{J0}|$, whereas $C_v = 585$ for $|U_{J1}|$. In terms of amplitude for maximal measured voltage 0.5V, we obtain $d_{Z-non} = 294.5\,nm$ and $d_{Z-mod} = 292.5\,nm$. The results are in very good agreement. Using the proportional constant e.g. $C_v = 589$; the amplitude of vibrations is at 0.4V is $d_Z = 235.6\,nm$. The same procedure was done for blue point. There the proportional constants are $C_v = 141$, $C_v = 136$ for $|U_{J0}|$, $|U_{J1}|$, respectively, which corresponds to maximal amplitudes of vibrations $d_{Z-non}(u = 0.5) = 70.5\,nm$ and $d_{Z-mod}(0.5) = 68\,nm$. This analysis only proves (13) and the reliability of the frequency modulated time average holography, but says nothing about the sensitivity of different orders *n* for the small amplitudes.

For that we plotted magnitude values along pixels denoted by the red line as outlined in the very top magnitude maps in the black frame of Fig. 3. The cross-section is chosen to be in a nearness of a nodal line, where the amplitude is minimal and tends to evince linear behavior. In the right hand side graph

denoted by (A) in Fig. 3, magnitude values of non-modulated technique (m=0) are plotted as a red circles. The green solid line represents theoretically predicted values. The measured magnitudes are scattered around the theoretical curve, moreover, the small range of the graph testifies about low sensitivity of measurement in this range. The same results are plotted in the right hand side graph (B) for frequency modulated measurement (n=1). The reconstructed magnitude values reliably follow the predicted curve. From the comparison of the both plots follows that the modulated technique brings much better sensitivity in case of very small amplitudes.

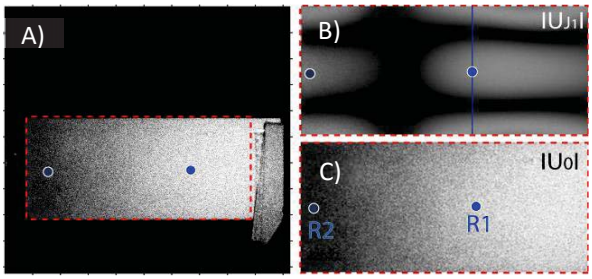

Fig. 4 (A) The overall field of view in image plane with steady cantilever recorded by digital holography. Red dashed line delineates ROI; (B) magnitude distribution within ROI of oscillating cantilever. Blue line denotes cross-section used for further analysis. Blue and violet points (pixels) are also important due to their detailed investigation; (C) magnitude distribution of steady cantilever within ROI with the two important points R1 and R2

In order to determine the smallest measurable amplitude by the frequency modulated holography (for our holographic arrangement); the following experiment was carried out. The supply voltage was successively increased started at 0 V with fine steps 0.05 mV up to 4 mV. Such low supply voltage generates extremely small amplitudes of vibration. The aim was to find the threshold of the supply voltage (or vibration amplitude) where noise represses measured signal and measurement can no longer be considered as valid. Again, two representative pixels (blue and violet points in Fig. 4) were chosen for detailed analysis. The graphically interpreted results of blue point are plotted in Fig. 5. The graph (A) represents coarse measurement executed in higher supply voltage range. The "coarse" measurement serves for calibration of independent (x) axis scale in order to obtain dependence on argument of Bessel function $\Omega = \frac{4\pi}{\lambda} d_z$ instead of supply voltage. This can be achieved with the use of properties of the first order Bessel function $J_{1-max}(\Omega = 1.84) = 0.58$. One should note, that for small amplitudes where $\Omega < 0.5$ the Bessel function can be approximated by linear function $J_1(\Omega) \approx \frac{1}{2}\Omega$, see red line in Fig. 5 (A). Finally, the graph (B) shows results of the "fine" measurement in the very small interval of supply voltages (small amplitudes). When approaching zero, the measured values (blue circles) do not significantly deviate from theoretical value up to $|U_{J1}|$~0.001. This was considered as the measurement threshold. Using the linear approximation $d_z = 2\frac{\lambda}{4\pi}|U_{J1}|$, the smallest measureable amplitude reaches d_z~0.085 nm or in terms of wavelength $d_z \sim \frac{\lambda}{6000}$.

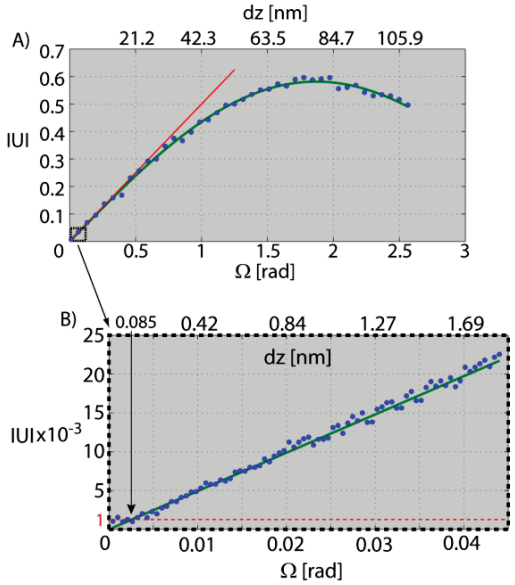

Fig. 5 (A) Coarse measurement of magnitude $|U_{J1}|$ at point R1 with increasing supply voltage. The independent axis is calibrated to argument of the Bessel function and out-of-plane deviation d_z. (B) Measured values at very small amplitudes of vibration, see black frame in (A). The red dashed line marks out the noise level and the lowest measurable amplitude

The level of noise presented in the reconstructed magnitude at this limiting value is around 20%, see Fig. 6 – blue circles. The amount of noise was computed as a mean $\langle \frac{|U_{J1}|}{\langle |U_{J1}| \rangle} \rangle$ of ratio of the measured magnitudes $|U_{J1}|$ and theoretical data represented by the average $\langle |U_{J1}| \rangle$ along the cross-section denoted by the blue line in Fig. 4 (B).

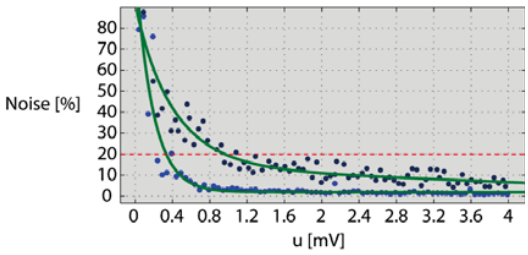

Fig. 6 Presence of noise in magnitude values in blue and violet point as a function of supply voltage (or amplitude of vibrations)

The theoretical value was estimated from magnitudes at large amplitudes and scaled linearly with respect to supply voltage, see Fig. 7. The theoretical value $\langle |U_{J1}| \rangle$ is denoted by red dashed line while the solid lines represent values of $|U_{J1}|$ at different supply voltages.

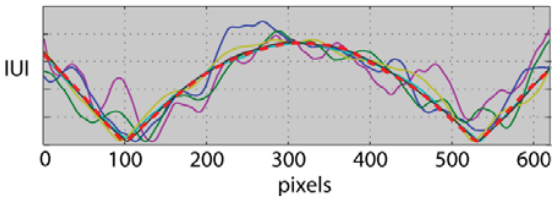

Fig. 7 Values of magnitude along the "blue" cross-section in Fig. 4. Dashed red line represents theoretical data, while solid lines represent values at different supply voltages (amplitudes of vibrations). For small amplitudes of vibrations the deviation from the theoretical curve rises (blue and purple curve) while larger amplitudes of vibrations result in better SNR (yellow). The limiting acceptable value of noise in data was set to be 20%

All the values plotted in Fig. 7 are normalized. As long as the supply voltage increases, the curves approach the theoretical value. This tendency can be approximated by decreasing exponential function (green line in Fig. 6), which reflects the probability density distribution of speckle noise $p(I) = exp(-\frac{I}{\langle I \rangle})$, where I denotes intensity and $\langle I \rangle$ is its average. It illustrates the fact, that speckle noise plays a crucial role in coherent measurement techniques like TADH.

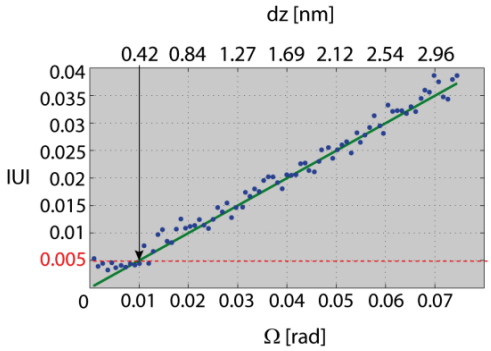

Fig. 8 Values of magnitude at violet point with increasing supply voltage. The independent axis is calibrated to argument of the Bessel function. The red line marks out the noise level and the lowest measurable amplitude

The same measurement procedure was repeated for pixel denoted by the violet circle. As it is shown in Fig. 8, the smallest measureable amplitude is five times greater when compared with the blue point: d_z~0.42 nm. The worse SNR can also be noticed in Fig. 6 (see the violet circles). At first sight it seems to be in contrary with the "blue point" measurement; however, subsequent analysis will clarify the apparent discrepancy.

Starting with the formula of the reconstructed magnitude field $|U_{J1}(R)| = |U_0(R)||J_1(\Omega(R))|$, where the magnitude distribution of non-oscillating object $|U_0(R)|$ is modulated by the first order Bessel function. Using $d|U_{J1}(R)|/dd_z$ one can define a sensitivity S of the frequency modulated time average holography:

$$S(R) = \frac{2\pi}{\lambda}|U_0(R)|\left(\left|J_0\left(\frac{4\pi}{\lambda}d_z(R) - B\right)\right| - \left|J_2\left(\frac{4\pi}{\lambda}d_z(R) - B\right)\right|\right). \quad (14)$$

The sensitivity of the time average holography is defined by wavelength, the average exposure determining $|U_0(R)|$ and the amplitude of vibrations change itself coded in an argument of the zeroth and the second order Bessel functions. For extremely small amplitudes $J_0(\Omega(R)) \approx 1$ and $J_2(\Omega(R)) \approx 0$; the formula (14) simplifies to

$$S(R) \approx \frac{2\pi}{\lambda}|U_0(R)|. \quad (15)$$

which is in agreement with linear approximation used earlier. The wavelength of the laser is very stable and spatially independent. On the other hand, the average exposure $|U_0(R)|$ varies with position R. The discrepancy present between the measurements at the blue and the violet point can be explained by the term $|U_0(R)|$. The normalized value of $|U_0|$ at the blue point $R1$ is $|U_0(R1)| = 1$, while $|U_0(R2)| = 0.25$ at the violet point $R2$. This results in ratio 5:1. Since the measurement in $R1$ gives the best SNR in the whole reconstructed field, the limiting value $|U_{J1}(R1)|$~0.001 can be considered as a spatially independent constant of the noise threshold $\Delta|U_{J1}|$ reachable in our experimental arrangements. The minimal measurable amplitude in position R2: $d_{Z-MIN}(R2) = \frac{\lambda}{2\pi}\frac{\Delta|U_{J1}|}{|U_0(R2)|} = \frac{\lambda}{2\pi}\frac{\Delta|U_{J1}|}{0.25} = 5\frac{\lambda}{2\pi}\Delta|U_{J1}|$ is therefore expected to be five times larger than in R1, as verified experimentally. It is worth noticing that the exposure $|U_0(R)|$ depends on the power of the laser, reflectivity and roughness of the object, dimensions of the object, geometrical arrangements etc. and therefore the noise threshold varies with these parameters. The noise threshold thus slightly varies for different objects under investigation

IV. Conclusion

This paper introduces some developments in the field of TADH. Different frequency shifts of the object and the reference wave in the experimental arrangements results in temporally harmonic variation of intensity values within digital hologram. When frequency of the reference wave is shifted by an integer multiple of frequency at which the object oscillates, the measurement range of the method can be shifted either to smaller or larger vibration amplitudes. Moreover, phase modulation can add a well-defined bias to the argument of the Bessel function. This can be used for the direct application of the phase-shifting technique. The combination of both approaches results in a rapid, accurate, robust and user-friendly method with ultimate dynamic range and evaluation of amplitude distribution independently in every pixel. We have experimentally proved the better performance of PMFSTADH over the classical TADH in the range of small amplitudes. The threshold of the smallest measurable amplitude is experimentally established to be under 0.1 nm or $\lambda/6000$.

REFERENCES

[1] R. L. Powell and K. A. Stetson, "Interferometric Vibration Analysis by Wavefront Reconstruction," *J. Opt. Soc. Am.*, vol. 55, no. 12, p. 1593, Dec. 1965.
[2] K. A. Stetson and R. L. Powell, "Interferometric Hologram Evaluation and Real-Time Vibration Analysis of Diffuse Objects," *J. Opt. Soc. Am.*, vol. 55, no. 12, p. 1694, Dec. 1965.
[3] J. W. Goodman, "Temporal Filtering Properties of Holograms," *Appl. Opt.*, vol. 6, no. 5, p. 857, May 1967.
[4] C. C. Aleksoff, "Temporally modulated holography," *Appl. Opt.*, vol. 10, no. 6, pp. 1329–1341, 1971.
[5] M. Ueda, S. Miida, and T. Sato, "Signal-to-noise ratio and smallest detectable vibration amplitude in frequency-translated holography: an analysis," *Appl. Opt.*, vol. 15, no. 11, pp. 2690–2694, 1976.
[6] P. Picart, J. Leval, D. Mounier, and S. Gougeon, "Time-averaged digital holography," *Opt. Lett.*, vol. 28, no. 20, pp. 1900–1902, Oct. 2003.
[7] F. L. Clerc, L. Collot, and M. Gross, "Numerical heterodyne holography with two-dimensional photodetector arrays," *ArXiv11125080 Phys.*, Dec. 2011.
[8] F. Joud, F. Laloë, M. Atlan, J. Hare, and M. Gross, "Imaging a vibrating object by Sideband Digital Holography," *Opt. Express*, vol. 17, no. 4, p. 2774, Feb. 2009.
[9] P. Psota, V. Ledl, R. Dolecek, J. Erhart, and V. Kopecky, "Measurement of piezoelectric transformer vibrations by digital holography," *IEEE Trans. Ultrason. Ferroelectr. Freq. Control*, vol. 59, no. 9, pp. 1962–1968, Sep. 2012.
[10] N. Verrier and M. Atlan, "Absolute measurement of small-amplitude vibrations by time-averaged heterodyne holography with a dual local oscillator," *Opt. Lett.*, vol. 38, no. 5, pp. 739–741, Mar. 2013.
[11] D. N. Borza, "Mechanical vibration measurement by high-resolution time-averaged digital holography," *Meas. Sci. Technol.*, vol. 16, no. 9, p. 1853, 2005.
[12] K. A. Stetson and W. R. Brohinsky, "Fringe-shifting technique for numerical analysis of time-average holograms of vibrating objects," *J. Opt. Soc. Am. A*, vol. 5, no. 9, pp. 1472–1476, Sep. 1988.
[13] P. Psota, V. Lédl, P. Vojtíšek, J. Václavík, R. Doleček, and P. Mokrý, "Advanced time average holographic method for measurement in extensive vibration amplitude range with quantitative single-pixel analysis," 2015, vol. 9508, p. 95080N–95080N–9.
[14] T. Kreis, *Handbook of holographic interferometry: optical and digital methods. 2005*. Weinheim: Wiley-VCH. xii